Design of a New Multispectral Waveform LiDAR Instrument to Monitor Vegetation

Zheng Niu, Zhigang Xu, Gang Sun, Wenjiang Huang, Li Wang, Mingbo Feng, Wang Li, Wenbin He, and Shuai Gao

***Abstract*—A multispectral full-waveform light detection and ranging (LiDAR) instrument prototype with four wavelengths and a supercontinuum laser as a light source was designed to monitor the fine structure and the biochemical parameters of vegetation. Components of the instrument included a 2-D scanning platform, a supercontinuum laser source, a receiving optical system, and a multichannel full-waveform measurement module. The LiDAR instrument can simultaneously measure multichannel-returned full-waveform laser signals. Position information in the recorded waveform allowed us to compute the distance from the target, whereas the intensity of the signal provided the spectral reflectance. Performance for the measuring distance and the spectrum was evaluated. Experiments indicated that the instrument has high measurement accuracy and has the ability to detect the biochemical characteristics of vegetation via construction of the normalized difference vegetation index and the photochemical reflectance index. The experiment also indicated that the instrument has the potential to generate spectral 3-D point clouds. Therefore, the instrument could play a significant role in detecting the vertical distribution of structural and biochemical characteristics of vegetation.**

***Index Terms*—Biochemical, full waveform, light detection and ranging (LiDAR), multispectral, vegetation.**

I. Introduction

VEGETATION ecosystems play important roles in global climate change, carbon uptake, ecological balance, and so on. In general, vegetation ecosystem consists of a variety of different types of species in the vertical direction such as high trees, low shrubs, and grass, leading to distinct vertical stratification characteristics. In a similar manner, structure and biochemical components present a vertical stratification distribution. Vertical distribution characteristic detection is an important prerequisite for accurate assessments of energy, water, and nutrient flows. Although the inversion result of structural and biochemical parameters has a high estimation accuracy for horizontal distributions, it is difficult to obtain a vertical distribution for parameters such as leaf area density and biochemical components using passive optical remote sensing [1].

Light detection and ranging (LiDAR) has the advantage of a high spatial resolution, an anti-interference ability, and a high detection sensitivity. As an active remote sensing technology, LiDAR is minimally influenced by illumination condition or shadows. Terrestrial or airborne LiDAR instruments mainly use monochrome lasers to recode the intensity of received signals, as well as to provide accurate geometric information. Traditional single-wavelength LiDAR has been widely used in the estimations of individual tree height, biomass at the plot level, and forest vertical structures [2]. Of late, radiometric calibration techniques have significantly promoted the applications of intensity information [3], [4]. However, intensity information obtained for a target is influenced by many factors, including the laser's power, the transmitting distance, the incidence angle, the reflectivity of the target, and the absorption of the medium. Therefore, it is difficult to obtain biochemical components from single-wavelength LiDAR observations. Other studies have indicated that a combination of spectral information and LiDAR information can improve accuracy for extracting these parameters [5], [6].

A full-waveform LiDAR can record the entire returned laser pulse at a reliable sampling rate, even as an emitted laser pulse penetrates the vegetation canopy. Therefore, a waveform profile through the depth of the canopy can be generated. Vertical structure measurements of the forest canopy can be obtained using a waveform analysis [7]. Radiative transfer model and geometrical optic model simulations indicate that the changes in forest leaf area density, leaf angle, and biochemical composition can be explained using variations of the waveform [8], [9].

Currently, passive optical sensors are able to perform multispectral acquisitions, whereas active commercial LiDAR sensors perform measurements in a single wavelength. Both the spectral and range information of objects can be obtained simultaneously if multispectral LiDAR is developed. Spectral 3-D point cloud data $(x, y, z, R(\lambda))$ can also be generated using multispectral LiDAR scanning. Tan and Narayanan [10] developed a multiwavelength airborne polarimetric LiDAR for vegetation remote sensing. To validate the instrument's ability for canopy detection, backscattered polarimetric returns and cross-polarization ratios were obtained from a small forested area. Gong *et al.* [11] proposed multiwavelength vegetation

Manuscript received July 15, 2014; revised November 28, 2014 and February 14, 2015; accepted February 17, 2015. Date of publication March 18, 2015; date of current version June 5, 2015. This work was supported by the Major State Basic Research Development Program of China under Grant 2013CB733405 and by the National Natural Science Foundation of China under Grant 41301389 and Grant 41201345. *(Corresponding authors: Zhigang Xu and Gang Sun.)*

Z. Niu, Z. Xu, G. Sun, L. Wang, M. Feng, W. Li, and S. Gao are with the State Key Laboratory of Remote Sensing Science, Institute of Remote Sensing and Digital Earth, Chinese Academy of Sciences, Beijing 100101, China (e-mail: imdr@163.com; sungang@radi.ac.cn).

W. Huang is with the Laboratory of Digital Earth Sciences, Institute of Remote Sensing and Digital Earth, Chinese Academy of Sciences, Beijing 100094, China.

W. He is with the College of Computer Science and Technology, Dongguan University of Technology, Dongguan 523106, China.

Color versions of one or more of the figures in this paper are available online at http://ieeexplore.ieee.org.

Digital Object Identifier 10.1109/LGRS.2015.2410788

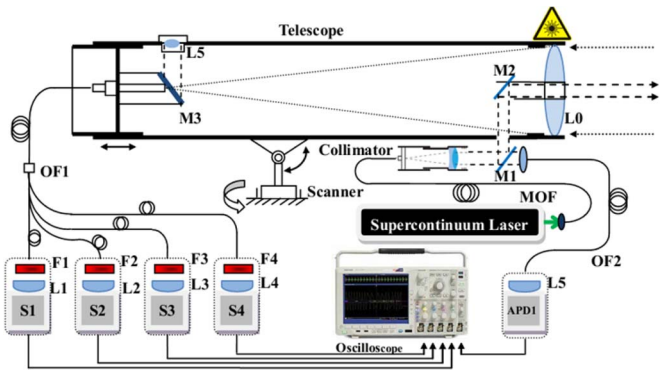

Fig. 1. Schematic of the LiDAR instrument.

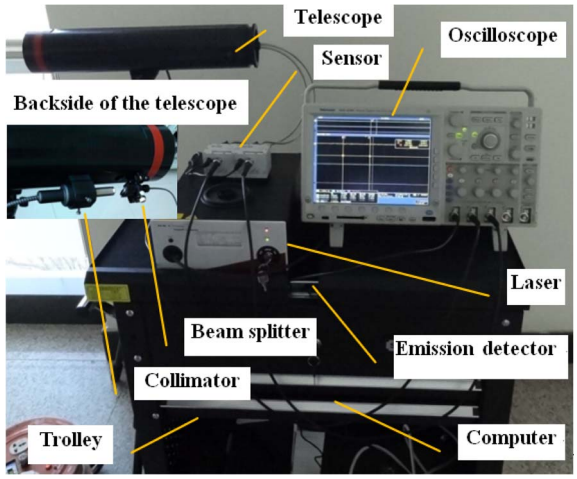

Fig. 2. Prototype of the multispectral waveform LiDAR instrument.

canopy LiDAR (MWCL) using continuous lasers with four wavelengths for vegetation classification. Woodhouse *et al.* [12] and Wallace *et al.* [13], reporting a multispectral canopy LiDAR system based on photon counting and a tunable laser, indicated that measurements of vegetation indices can be produced along the laser profile. The instrument was later improved using a supercontinuum laser source and a small conifer sample was scanned to extract full-waveform data at four wavelengths [14]. Chen *et al.* [15] built a two-channel LiDAR to show its potential application of distinguishing the normalized difference vegetation index (NDVI) for Norway spruce. Hakala *et al.* [16] built a system using eight wavelength avalanche photodiode detectors to conduct laboratory measurements and generated 3-D point clouds with reflectance and specific vegetation indices. Previous researches have shown the great potential for obtaining vertical distribution information for vegetation parameters.

This letter provides a new design for a four-wavelength full-waveform LiDAR instrument prototype that can simultaneously measure the range and spectrum of objects. Experiments were conducted to evaluate its accuracy for range measurements and its capability to acquire spectra.

II. Description of the System

The multispectral waveform LiDAR system proposed in this letter is composed of the following subsystems (see Fig. 1): 1) a 2-D scanning platform; 2) a supercontinuum pulsed laser source; 3) a coaxial optical transmitting and receiving system fixed to the scanning platform; 4) a full-waveform multichannel data acquisition system; and 5) a control center. The pulsed supercontinuum laser (NKT Photonics) with a spectral range of 450–2400 nm produces a ∼1- to 2-ns pulse at a repetition rate of 24 kHz. Broadband light emitted by the laser is collimated (the divergence angle is less than 5 mrad) when passing through the refracting collimator. The collimated beam is reflected twice by two mirrors (M1 and M2) and transmitted into the optical axis of the telescope. The mirror M1 is also used as a beam sampler plate for transmitting a small portion of emitted light through an optical fiber to the avalanche photon diodes (APD1) detection sensor. The APD1 sensor is used to collect a sample of the emitted laser waveform and the emitted signal is used to trigger a measurement for capturing the waveforms of both the emitted pulse signal and the echoes.

An achromatic refractor telescope (with a 400-mm focal length and an 80-mm aperture diameter) collects the returned laser echoes. To separate the receiving light into four channels, a beam splitter optical fiber is placed at the focal point of the telescope. Light then passes through the bandpass filters (F1, F2, F3, and F4) and was split into four separate wavelengths. Light emitted from the fiber is then imaged onto four detectors (S1, S2, S3, and S4) through the convergence lens (L1, L2, L3, and L4). The bandpass filters include narrowband interference filters with center wavelengths at 531, 570, 670, and 780 nm, and a bandwidth of 10 nm. As for the detectors, four avalanche diode modules (MenloSystems APD, with sensitive wavelengths of ∼400 to 1000 nm, bandwidths of 1 MHZ to 1 GHz, and a rise time of 0.5 ns) convert the laser echo into an electronic analog signal. Output signals of the detector are sampled and recorded using a high-speed oscilloscope (Tektronix MSO4104, 5 GHz sampling rate, 1 GHz bandwidth, and four analog channels) and a set of high-resolution echo waveforms is produced. A prominent feature of the receiving system is the introduction of a Pritchard aiming system to assure that the target is targeted accurately. A 45° mirror M3 is fixed at the focal point of the telescope. A 2 mm hole at the center of the mirror M3 produces a field of view (FOV) of ∼4 to 5 mrad, the FOV corresponding to the measured target. Light projected out of the hole of the reflection mirror represents the surroundings of the target field. The light is then reflected by a 45° mirror to eyepiece L5, where a black spot corresponding to the 2-mm hole superimposes the image of the surroundings. The black spot represents an accurate measurement position of the object, indicating that the target is aimed 100%. The photograph of the prototype system is provided in Fig. 2.

The prototype system is equipped with a beam splitter optical fiber and narrow bandpass filters. Wavelength characteristics of the system can be modified by changing the filter to adapt to different experiments. In the system, 531 and 570 nm can be used to calculate the photochemical reflectance index (PRI) [17]. Wavelengths of 670 and 780 nm can be used to determine the normalized difference vegetation index (NDVI). The prototype system can measure both flight time and reflectance through the postprocessing of recorded waveforms for each channel.

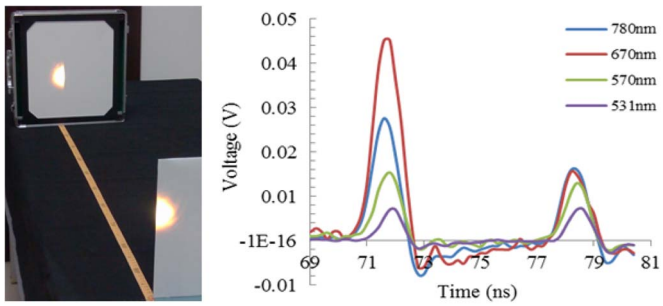

Fig. 3. Ranging experiment. (a) A photograph showing the laser transmitting through two diffuse reflectors with interdistance of 1 m. (b) Raw waveforms obtained from the two reflectors at four wavelengths.

TABLE I
LIDAR RANGE MEASUREMENT RESULT CALCULATED BY THE 670 nm CHANNEL

Range (m)	Mean (mm)	Max (mm)	Standard Deviation (mm)	Difference (mm)
1	1009.4	995.3	1025.3	8.9
2	2008.7	1990.1	2022.9	10.4

III. DESCRIPTION OF THE SYSTEM

Preliminary experiments were conducted in the laboratory of the Institute of Remote Sensing and Digital Earth from November 2013 to March 2014. The ranging test was designed to evaluate the capability of ranging based on the time-of-flight method. The feasibility of simultaneous measurements for distance and spectra was demonstrated through the spectrum tests.

A. Ranging Experiment

Ranging accuracy and resolution are important technical indicators for LiDAR. Two experiments were designed and performed. The purpose of experiment one was to evaluate the accuracy of the measured distance. Referring to the methods provided in [10] and [15], two diffuse reflectors were placed ∼10 m from the instrument. The distance between the two reflectors was 1 and 2 m, respectively. Half of the laser spot was separately reflected by the two reflectors; therefore, two adjacent Gaussian pulses were formed within the returned waveform. The distance between the two reflectors was obtained by calculating the time difference between the two Gaussian peaks.

The setup for reflectors with the ranging experiment is provided in Fig. 3(a), and the four waveforms captured are provided in Fig. 3(b).

The time difference of the two echo peaks (670 nm) was measured. Distance was calculated based on the time-of-flight method.

As shown in Table I, the average distance between laser radar measurements was 1009.4 and 2008.7 mm, respectively. The precision of ranging (standard deviation) was 10.4 mm.

TABLE II
RESOLUTION OF RANGING CALCULATED BY THE 670 nm CHANNEL

Relative Range (mm)	Time difference (ns)	Range calculated by time-of- flight (mm)	Error (mm)
500	3.37	506.10	6.10
400	2.70	404.73	4.73
300	2.00	300.10	0.10
200	1.36	203.56	3.56
150	0.79	119.10	-30.90

A certain bias existed between the measured and the actual distance. Possible reasons are given in the following.

1) The sampling rate of the oscilloscope was 5 G/s with an interval of 0.2 ns; therefore, the theoretical ranging resolution was 30 mm. The maximum corresponding digitized random measurement error was also 30 mm.
2) The flight time was calculated based on waveforms stored within the oscilloscope, which might have errors in calculating the interval time.
3) The placement angle of the two reflectors may not be perfectly perpendicular to the direction of light and a slight distortion of the waveform was formed.

For multispectral LiDAR, the relative distance between two targets can be obtained by calculating the time difference between two echo peaks of any wavelength. With the increase of wavelength, the echo arrival time occurred in advance. Asynchronization was shown between different wavelengths. The time difference of the peaks was ∼0.7 ns for wavelengths at 780 and 531 nm. Such asynchronization is mainly caused by the inherent characteristics of the supercontinuum laser source, indicating that each wavelength is not strictly synchronized with slightly different timing at the beginning of transmission. With an increase in wavelength from 480 to 800 nm, the maximum delayed time of the pulse was ∼700 ps.

The second purpose of the ranging experiment was to test the capability for distinguishing adjacent objects. The experiment was accomplished by keeping one reflector fixed and adjusting the second reflector to approach the fixed reflector. When two echo peaks were not distinguished from the waveform, the distance was determined to be the minimum range resolution. In this experiment, the distance between the two reflectors was set to 500, 400, 300, 200, and 150 mm, respectively. The range resolution calculated at 670 nm is shown in Table II.

When the distance between two reflective plates was less than 150 mm, double peaks could not be obviously observed from the waveforms. A decomposing method could then be used to calculate the position of the two peaks [16].

B. Spectral Experiment

The multispectral LiDAR produced a pulsed broadband laser footprint through use of cascaded nonlinear optical interactions within the optical fiber. The spectral information of the observed object could be detected using intensity information obtained from a set of waveform echoes. By constructing the spectral vegetation indices and to evaluate the system's ability

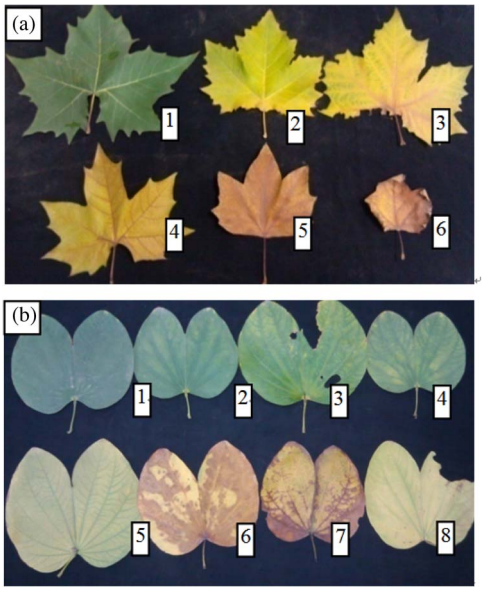

Fig. 4. Leaves tested. (a) Leaves of Platanus. (b) Leaves of Bauhinia flowers.

for classification using LiDAR spectra, the tests were used to monitor vegetation. In the experiment, two groups, that is, group one (670 and 780 nm) and group two (531 and 570 nm), were selected for calculating dual-band vegetation indices NDVI and PRI. Six different leaf spectra, with a size of 12 cm × 12 cm of Platanus [see Fig. 4(a)] were acquired on 14 Nov, 2013. The index was labeled from 1 to 6 based on greenness. Eight different leaf spectra, with a size of 11 cm × 11 cm, of the Bauhinia flower [see Fig. 4(b)] were acquired on 27 March, 2014 in the city of Dongguan, China. The index was labeled from 1 to 8 based on greenness.

The workflow of the experiment was as follows.

1) A whiteboard was placed ∼10 m from the laser source. Emitted and reflected waveforms obtained from the whiteboard were measured separately as the referring waveform. The diameter of the footprint was ∼5 cm.
2) Leaves with various levels of greenness were placed on the board and measured separately and reflected waveforms were measured and recorded. Each leaf was measured ten times.
3) Because of the slight variations of emitted laser energy (the stability of the laser pulse energy source was 0.25 dB for the NKT SuperK Compact), the returned waveform of the leaves was normalized according to the referring waveform introduced in Step 1. Normalization reduced the instability impact of the NKT SuperK Compact [15].
4) The reflectance of each leaf was used to calculate PRI and NDVI.

Meanwhile, a spectrometer (AVASpec-2048-USB2, Avantes Corp, Dutch) with a spectral range of ∼200 to 1100 nm and a spectral resolution of 1.4 nm at ∼300 to 1100 nm was used for measuring the reflected spectrum of the corresponding leaves. Measurements were performed at ∼14:00 (local time) on a sunny day. For measurements, leaves were placed flat on the ground and the fiber head was placed downward from the leaf

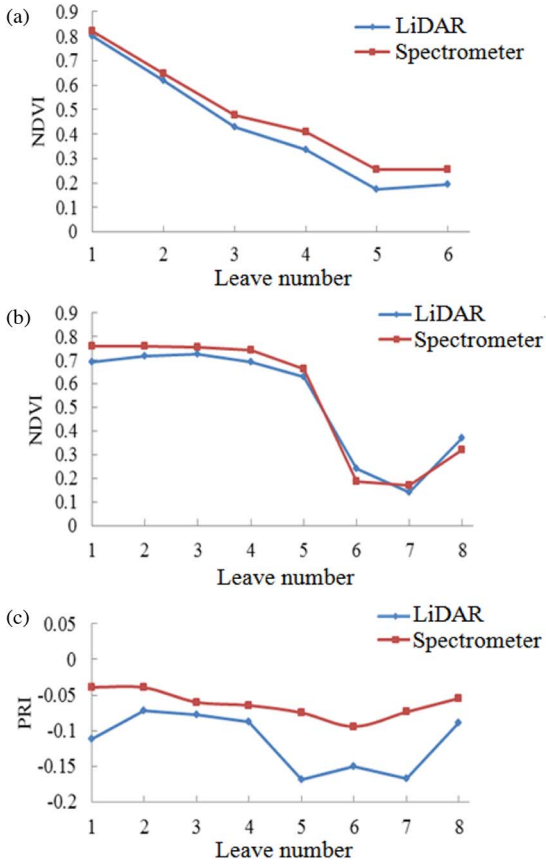

Fig. 5. Comparison between vegetation indices measured by LiDAR instrument and the spectrometer. (a) A comparison chart of the NDVI of the Platanus; (b) A comparison chart of the NDVI of the Bauhinia flower; (c) A comparison chart of the PRI of the Bauhinia flower.

at approximately 10 cm. The FOV of the optical fiber probe was only ∼25°. Therefore, the diameter of the footprint on the observed target was ∼5 cm. The area of spectrometer detection and the footprint of the laser spot were basically the same.

Following the experiment, reflectance at four wavelengths was extracted. Indices obtained by the spectrometer were then compared with those obtained from the LiDAR instrument. Experimental results of NDVI obtained for Platanus are provided in Fig. 5(a) and those obtained from Bauhinia flowers are provided in Fig. 5(b). Results on PRI obtained for Bauhinia flowers are provided in Fig. 5(c).

Fig. 5(a) and (b) indicates that the NDVI value obtained from the spectrometer generally agreed well with values obtained from the multispectral LiDAR instrument. The relationship between them for the Platanus was as follows: $\mathrm{NDVI}_{\mathrm{Spectrometer}} = 0.908 \times \mathrm{NDVI}_{\mathrm{LiDAR}} + 0.090$, $R^2 = 0.998$, and $\mathrm{RMSE} = 0.007$. For the Bauhinia flower, the relationship was as follows: $\mathrm{NDVI}_{\mathrm{Spectrometer}} = 1.119 \times \mathrm{NDVI}_{\mathrm{LiDAR}} - 0.043$, $R^2 = 0.983$, and $\mathrm{RMSE} = 0.033$. Fig. 5(c) shows that the center wavelength and the bandwidth was important for the comparison because of the bandwidth difference between the LiDAR instrument (10 nm) and the spectrometer (1.4 nm). Therefore, the capability of this multispectral LiDAR instrument to detect the vegetation PRI may need further investigation. For Bauhinia flowers, the correlation between the values obtained from the two instruments was as

follows: $\text{PRI}_{\text{Spectrometer}} = 0.318 \times \text{PRI}_{\text{LiDAR}} - 0.026$, $R^2 = 0.485$, and $\text{RMSE} = 0.064$.

IV. Discussion

Our experiments indicate that more precise time and energy measurement systems with calibrations can improve measurement accuracy. Higher bandwidth (>2 GHz) oscilloscopes can reduce the deformation of the echo signal. Data acquisition system with a higher time resolution can provide flight time measurements more accurately. To achieve hyperspectral measurements, a grating method could be considered as a substitute for the current spectral filter. A Cassegrain telescope could also improve the efficiency of the optical system, increase the signal-to-noise ratio (SNR), and enlarge the measurement distance. Because of the inconsistencies of the supercontinuum laser pulse energy and inconsistencies in the sensitivity of the APD module, calibrations should be conducted in the future.

When the optical portion is driven by a two-axis rotary, the system can be configured to produce a 3-D point cloud, where each point has both a distance and a plurality of spectral band reflectivity information. The inversion of structural and biochemical parameters can be developed from 2-D to 3-D. However, both the instability of supercontinuum laser power and the small diameter of the refracting telescope may result in a lower receiving sensitivity and SNR. Additionally, the oscilloscope used for the high-speed analog/digital conversion and data collection may decrease the efficiency of the test in outdoor environments.

In the future, we will evaluate the system for the estimation of biochemical parameters for vegetation [18]. Our approach should be further verified using larger data sets and be extended to more complex conditions. Hyperspectral LiDAR with an extended distance and a wider spectral range will greatly improve the efficiency for monitoring the vertical distribution of vegetation parameters using remote sensing.

V. Conclusion

A four-wavelength multispectral LiDAR prototype system based on a supercontinuum laser source has been proposed. Distance and spectral experiments at the leaf scale were successfully performed. Based on the experiments, we determined that the multispectral LiDAR instrument could simultaneously obtain range and spectral information. Performance for measuring distance can meet the requirements for vertical stratification and detection. Spectral information extracted from the echo waveform helps to describe vegetation more accurately. The instrument also has the potential to generate 3-D point clouds with spectral information and 3-D information related to vegetation growth conditions.

Acknowledgment

The authors would like to thank the efforts of reviewers in improving the quality of this manuscript.

References

[1] H. Tang *et al.*, "Retrieval of vertical LAI profiles over tropical rain forests using waveform lidar at La Selva, Costa Rica," *Remote Sens. Environ.*, vol. 124, pp. 242–250, Sep. 2012.

[2] M. van Leeuwen and M. Nieuwenhuis, "Retrieval of forest structural parameters using LiDAR remote sensing," *Eur. J. Forest Res.*, vol. 129, no. 4, pp. 749–770, Jul. 2010.

[3] F. Coren and P. Sterzai, "Radiometric correction in laser scanning," *Int. J. Remote Sens.*, vol. 27, no. 15, pp. 3097–3104, Aug. 2006.

[4] W. Wagner, "Radiometric calibration of small-footprint full-waveform airborne laser scanner measurements: Basic physical concepts," *ISPRS J. Photogramm. Remote Sens.*, vol. 65, no. 6, pp. 505–513, Nov. 2010.

[5] E. Puttonen, A. Jaakkola, P. Litkey, and J. Hyyppä, "Tree classification with fused mobile laser scanning and hyperspectral data," *Sensors*, vol. 11, no. 5, pp. 5158–5182, May 2011.

[6] A. Swatantran, R. Dubayah, D. Roberts, M. Holton, and J. B. Blair, "Mapping biomass and stress in the Sierra Nevada using LiDAR and hyperspectral data fusion," *Remote Sens. Environ.*, vol. 115, no. 11, pp. 2917–2930, Nov. 2011.

[7] F. G. Hall *et al.*, "Characterizing 3D vegetation structure from space: Mission requirements," *Remote Sens. Environ.*, vol. 115, no. 11, pp. 2753–2775, Nov. 2011.

[8] W. Ni-Meister, D. L. B. Jupp, and R. Dubayah, "Modeling LiDAR waveforms in heterogeneous and discrete canopies," *IEEE Trans. Geosci. Remote Sens.*, vol. 39, no. 9, pp. 1943–1958, Sep. 2001.

[9] G. Sun and K. J. Ranson, "Modeling LiDAR returns from forest canopies," *IEEE Trans. Geosci. Remote Sens.*, vol. 38, no. 6, pp. 2617–2626, Nov. 2000.

[10] S. Tan and R. Narayanan, "Design and performance of a multiwavelength airborne polarimetric lidar for vegetation remote sensing," *Appl. Opt.*, vol. 43, no. 11, pp. 2360–2368, Apr. 2004.

[11] W. Gong *et al.*, "Multi-wavelength canopy LiDAR for remote sensing of vegetation: Design and system performance," *ISPRS J. Photogramm. Remote Sens.*, vol. 69, pp. 1–9, Apr. 2012.

[12] I. H. Woodhouse *et al.*, "A multispectral canopy LiDAR demonstrator project," *IEEE Geosci. Remote Sens. Lett.*, vol. 8, no. 5, pp. 839–843, Sep. 2011.

[13] A. Wallace, C. Nichol, and I. Woodhouse, "Recovery of forest canopy parameters by inversion of multispectral LiDAR data, " *Remote Sens.*, vol. 4, no. 2, pp. 509–531, Feb. 2012.

[14] A. M. Wallace *et al.*, "Design and evaluation of multispectral LiDAR for the recovery of arboreal parameters," *IEEE Trans. Geosci. Remote Sens.*, vol. 52, no. 8, pp. 4942–4954, Aug. 2014

[15] Y. Chen *et al.*, "Two-channel hyperspectral LiDAR with a supercontinuum laser source," *Sensors*, vol. 10, no. 7, pp. 7057–7066, Jul. 2010.

[16] T. Hakala, J. Suomalainen, S. Kaasalainen, and Y. Chen, "Full waveform hyperspectral LiDAR for terrestrial laser scanning," *Opt. Exp.*, vol. 20, no. 7, pp. 7119–7127, Mar. 2012.

[17] J. A. Gamon, L. Serrano, and J. S. Surfus, "The photochemical reflectance index: an optical indicator of photosynthetic radiation use efficiency across species, functional types, and nutrient levels," *Oecologia*, vol. 112, no. 4, pp. 492–501, Nov. 1997.

[18] W. Li, G. Sun, Z. Niu, S. Gao, and H. Qiao, "Estimation of leaf biochemical content using a novel hyperspectral full-waveform LiDAR system," *Remote Sens. Lett.*, vol. 5, no. 8, pp. 693–702, Sep. 2014.